Reinforcing hydrogels with *in situ* formed amorphous $CaCO_3$

*Huachuan Du, Tianyu Yuan, Ran Zhao, Matteo Hirsch, Michael Kessler, Esther Amstad**

Dr. H. Du, T. Yuan, R. Zhao, M. Hirsch, M. Kessler, Prof. E. Amstad
Soft Materials Laboratory, Institute of Materials, École Polytechnique Fédérale de Lausanne (EPFL), 1015 Lausanne, Switzerland
E-mail: esther.amstad@epfl.ch

Keywords: biomineralization, $CaCO_3$, hydrogels, mechanical properties, organic-inorganic hybrid composites

Mineralizing hydrogels with $CaCO_3$ is an attractive strategy to reinforce them, because of the excellent mechanical and biological properties of $CaCO_3$. Unfortunately, the degree of hydrogel reinforcement achieved with $CaCO_3$ remains limited. An important contributing factor is the poor control over the $CaCO_3$ formation that leads to an incomplete understanding of its reinforcing mechanism. To address this challenge, we systematically investigate the influence of the formation of $CaCO_3$ on the mechanical properties of a model hydrogel, poly(acrylamide) (PAM), that is reinforced by these minerals. We demonstrate that the amount, size, structure and morphology of $CaCO_3$ significantly influences the mechanical properties of mineralized hydrogels. For example, while the fracture energy of PAM hydrogels is increased 3-fold if reinforced with individual micro-sized $CaCO_3$ crystals, it increases by a factor of 13 if reinforced with a percolating ACC nano-structure that forms in the presence of a sufficiently high quantity of Mg^{2+} additives. These insights will likely enable a more targeted reinforcement of hydrogels with $CaCO_3$ by tuning the mechanical properties of the resulting composites over a much wider range than is currently possible.

1. Introduction

Hydrogels are three-dimensional polymer networks that are filled with a large amount of water.[1] They are attractive materials for a wide range of applications including regenerative medicine,[2] bioelectronics,[3] water treatment[4] and energy storage.[5] However, the poor mechanical properties of many hydrogels often limit their applications.[6] The mechanical properties of hydrogels can be improved by designing novel topological hydrogels that possess

more homogeneous networks.[7,8] Alternatively, they can be improved by incorporating energy dissipative domains,[6] such as sacrificial polymer chains,[9] inorganic mineral particles,[10,11] microgels,[12] and fibers,[13] on the molecular,[9,14] nanoscopic,[10,11,15] microscopic[12,16] and macroscopic[13] scales into conventional hydrogel networks. Among them, a particularly attractive means to reinforce hydrogels is the mineralization with $CaCO_3$:[17–20] This mineral is abundant in nature, easy to synthesize, possesses a tunable size, structure and morphology, and displays excellent mechanical properties, biocompatibility, biodegradability and bioactivity.[17,19,21–25]

Nature often uses $CaCO_3$ biominerals to mechanically reinforce soft organic tissues. The formation of $CaCO_3$ and thereby the size, structure, morphology and orientation of the resulting $CaCO_3$ biominerals are precisely controlled by the physicochemical properties of the tissue matrices and the presence of certain soluble additives, such as acidic proteins and Mg^{2+} ions.[26–28] As a result of this precise control, many $CaCO_3$-based biocomposites, such as nacre[29,30] and crustacean exoskeletons,[31] display fascinating mechanical properties. Inspired by the biomineralization strategy employed by nature, a variety of excellent examples to reinforce dry hard composites with $CaCO_3$ have been demonstrated.[32–34] By contrast, the biomineralization strategy has been rarely employed to reinforce soft hydrogels with $CaCO_3$,[17–20] despite the large number of studies devoted to the formation of micro-sized $CaCO_3$ single crystals within hydrogel matrices.[35] This shortcoming is likely related to the incomplete understanding of the influence of soluble additives and the composition of hydrogels, especially their functionalization with high affinity motives for $CaCO_3$ on the mechanical properties of mineralized hydrogels.

Systematic studies of the effect of minerals on the mechanical properties of reinforced hydrogels require a mineralization method that offers a tight control over the content, location, size and structure of $CaCO_3$. In addition, this method must be compatible with different soluble additives and functional groups present within the hydrogel. Currently available mineralization methods cannot simultaneously meet all these requirements. Soft matrices are frequently reinforced with $CaCO_3$ by immersing the hydrogel in a Ca^{2+} containing solution before CO_3^{2-} is introduced via the addition of another aqueous solution[36,37] or the diffusion of gases[32,38–40] to initiate the mineralization. Unfortunately, these methods often lead to an uncontrolled formation of minerals that are preferentially located at the surface of the matrices. This shortcoming can be addressed with the more recently introduced enzyme-induced mineralization where $CaCO_3$ homogeneously forms within the hydrogel. This is achieved by trapping urease, an enzyme that catalyzes the decomposition of urea and hence the production

of CO_3^{2-}, within the hydrogel.[17,18,41] However, the enzymatic activity and therefore the degree of mineralization strongly depend on the composition of the hydrogel and the mineralization solution, preventing systematic studies on the influence of soluble additives and functional groups present within the hydrogel on the mineralization. This shortcoming limits the choice of hydrogels and additives that can be used to control the mineralization. Moreover, while the possibility to control the mineral content in hydrogels by changing the mineralization time has been demonstrated in all the mentioned methods, the extent of this control is limited. To overcome these limitations and thereby to gain a better understanding of the reinforcement of hydrogels with $CaCO_3$, new mineralization methods that offer a tight control over the formation of $CaCO_3$ in the presence of different soluble additives and functional groups present within the hydrogel are required.

In this paper, we systematically study the influence of the formation of $CaCO_3$ on the mechanical properties of a model hydrogel, PAM. To achieve this goal, we introduce a modified gas-diffusion mineralization method to produce $CaCO_3$ that is uniformly distributed within PAM. Taking advantage of this feature, we demonstrate that especially the amount, size, structure, and morphology of $CaCO_3$ influences the mechanical properties of mineralized PAM. In particular, we demonstrate that hydrogels can be reinforced very efficiently with a percolating mineral network of amorphous calcium carbonate (ACC) nanoparticles that forms within the hydrogel if Mg^{2+} is present: The fracture energy of these hydrogels increases by a factor 13 while their stiffness increases 4-fold upon mineralization. We show that the stiffness of the hydrogel increases even more, by a factor 50, if PAM is functionalized with acrylic acid (AA) that strengthens the hydrogel-ACC interactions and controls the size and percolation of ACC nanoparticles . These results illustrate the potential to efficiently mechanically reinforce hydrogels with $CaCO_3$ by taking advantage of lessons learned from nature.

2. Results and discussion

2.1. Modified gas-diffusion mineralization method

Polyacrylamide (PAM) hydrogels are often employed as a model system to explore different reinforcing strategies.[9,11,14,42] To investigate the reinforcing effect of $CaCO_3$ on hydrogels, we therefore employ this hydrogel as the soft matrix. Unfortunately, the conventional gas-diffusion method that has often been used to conduct $CaCO_3$ mineralization in soft matrices[32,38–40] results in an uncontrolled formation of $CaCO_3$ layer on the surfaces of mineralized hydrogels. This mineral layer influences the mechanical properties of reinforced hydrogels, thereby hampering systematic studies on the formation of $CaCO_3$ on its reinforcing effect. To overcome this difficulty, we modify this gas-diffusion method: We dissolve $CaCl_2$ in an acrylamide (AM)

monomer solution before we crosslink the monomers using UV light, as schematically illustrated in **Figure 1a**. To initiate the mineralization, we expose the crosslinked $CaCl_2$-containing hydrogels to ammonium carbonate powder that decomposes into CO_2 and ammonia. The $CaCl_2$-containing PAM hydrogels are initially transparent and become white after 4 days of incubation, as shown in **Figure 1b** and **1c**. These results indicate that $CaCO_3$ particles that randomly scatter light form within $CaCl_2$-containing hydrogels. To determine the structure of the formed $CaCO_3$ particles, we perform X-ray diffraction (XRD) and Fourier-transform infrared spectroscopy (FTIR) on the samples. The $CaCO_3$ particles are composed of vaterite and calcite, two anhydrous crystalline polymorphs of $CaCO_3$, as shown in **Figure S1** and **S2**. To test if our method indeed avoids the uncontrolled formation of $CaCO_3$ layers on the PAM hydrogel surface, we visualize the cross-section of the mineralized PAM hydrogel using scanning electron microscopy (SEM) and characterize its composition with Energy-dispersive X-ray spectroscopy (EDX). We observe uniformly distributed $CaCO_3$ crystals throughout the sample and do not find any obvious sign of mineral surface layers, as exemplified in **Figure 1d**, **1e** and **S3**. These results indicate that our method homogeneously mineralizes hydrogels without depositing undesired mineral layers on their surfaces.

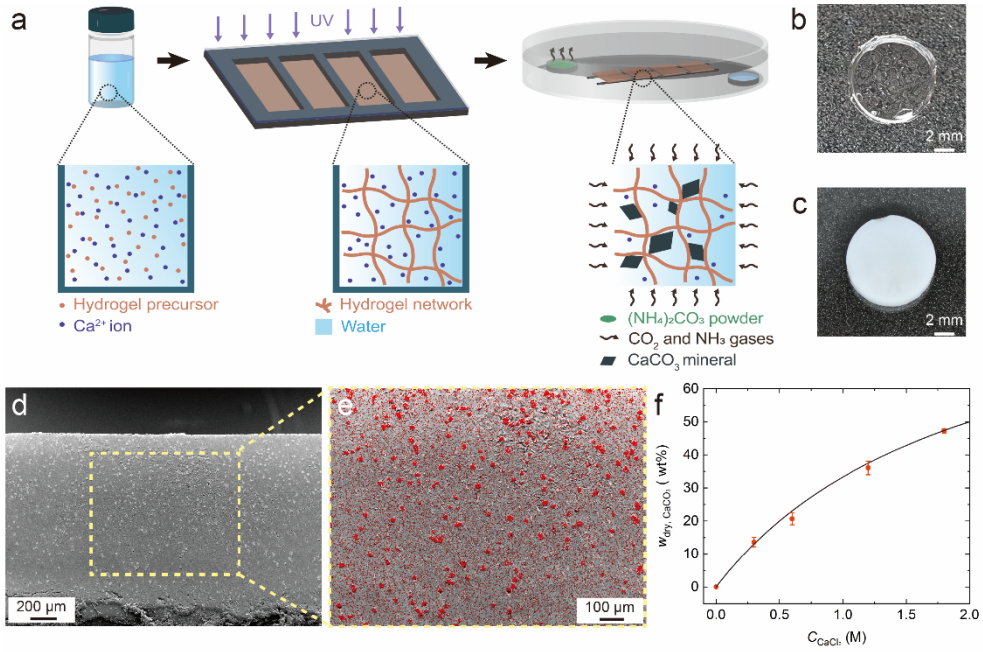

Figure 1. Mineralization of PAM hydrogels with $CaCO_3$. (a) Schematic illustration of the preparation of PAM hydrogels mineralized with $CaCO_3$. (b-c) Photographs of the $CaCl_2$-containing PAM hydrogel (b) before and (c) after mineralization. (d) SEM images of the polished cross-section of a mineralized PAM hydrogel. (e) SEM image of the region marked with the rectangle in (d) overlayed with the Ca element map obtained using EDX. (f) Weight fraction of $CaCO_3$ crystals ($W_{dry,CaCO3}$) in the dry hydrogel as a function of the initial $CaCl_2$

concentration. Values measured with TGA are indicated with red dots and the theoretical values calculated by assuming a complete conversion of $CaCl_2$ into $CaCO_3$ are indicated with the black line.

Our samples are prepared by pre-mixing well-defined concentrations of $CaCl_2$ and AM monomers. We therefore expect the mineral content contained in the hydrogels to be only determined by the initial ratio of $CaCl_2$ to monomer. To verify this expectation, we vary the initial concentration of $CaCl_2$ from 0.3 to 1.8 M while keeping the monomer content constant and quantify the weight fractions of $CaCO_3$ contained in the dry mineralized hydrogels using thermogravimetric analysis (TGA), as detailed in **Figure S4**. With increasing amount of added $CaCl_2$, the $CaCO_3$ content within the dry hydrogels increases from 13.6 ± 1.5 wt% to 47.4 ± 0.7 wt%. This result is in good agreement with the theoretical values calculated by assuming a complete conversion of $CaCl_2$ into $CaCO_3$, as shown in **Figure 1f**. Hence, our modified gas-diffusion mineralization method offers a precise control over the $CaCO_3$ mineral content within hydrogels.

2.2. Influence of $CaCO_3$ crystal content

The extent of mechanical reinforcement of the hydrogel obtained with fillers often depends on the filler content.[10,11,15] To study how the amount of $CaCO_3$ contained in our hydrogels influences their mechanical properties, we measure their Young's moduli (E) as a function of the volume fraction of $CaCO_3$ contained in them using tensile tests. The Young's modulus of these hydrogels increases with increasing mineral content, as shown in **Figure 2a** and **S5a**, indicating that the formed $CaCO_3$ crystals stiffen the hydrogels. To determine the reason for this stiffening, we compare our Young's moduli with those predicted by the Guth-Gold model for non-interacting filler particles.[42,43] The Guth-Gold model predicts the E of hydrogels containing 8.0 vol% $CaCO_3$, corresponding to those produced from a monomer solution containing 1.8 M, to be 30 kPa $CaCl_2$, as detailed in **Figure S6**. We obtain a much higher E of 54.0 ± 7.7 kPa, suggesting that the formed $CaCO_3$ crystals interact with the PAM hydrogel network. To investigate the nature of these interactions, we compare the FTIR spectra of neat PAM hydrogels with those containing $CaCO_3$ crystals. If hydrogels are mineralized with $CaCO_3$ crystals, the characteristic peak corresponding to the C=O stretching of PAM shifts from 1662 cm^{-1} to 1655 cm^{-1}, as shown in **Figure 2b** and **S2**. Similarly, the peak at 3200-3340 cm^{-1} corresponding to the N-H stretching of PAM splits into two peaks. These changes in the FTIR spectra imply that the formed $CaCO_3$ crystals chemically interact with the PAM hydrogel.[44,45] Particles that interact with hydrogels can often act as multivalent crosslinking points.[15,46] To

test if the formed $CaCO_3$ crystals provide any additional crosslinking sites for the PAM, we visualize the morphology of the organic/inorganic interfaces using SEM. Interestingly, the surfaces of $CaCO_3$ crystals are connected to the hydrogel matrix through many thin polymer fibers, as exemplified in **Figure 2c** and **S7**. These results suggest that the formed $CaCO_3$ crystals increase the crosslinking density of the PAM hydrogel and thereby significantly stiffen it.

Fillers that interact with the hydrogel often increase its toughness.[11,15,47] To test if this is also the case for our hydrogel, we carry out single-edge notch tensile tests on them.[14] Indeed, notched mineralized hydrogels display larger critical extensions that correspond to the crack initiation compared to the notched neat PAM hydrogels, as illustrated in **Figure 2d**. These results indicate that the interaction between $CaCO_3$ crystals and PAM hydrogels effectively delays the crack initiation. In addition, the notched mineralized hydrogels display a more progressive fracture upon crack propagation, which is likely attributed to the crack deflection or bridging caused by the same interaction.[48] To quantify the toughness of hydrogels, we calculate their fracture energy (Γ) using the tensile test results, as detailed in the **Figure S5**. While the neat hydrogels have Γ around 105.0 ± 23.5 J m^{-2}, hydrogels containing 1.2 vol% $CaCO_3$ crystals possess a Γ of 184.0 ± 22.8 J m^{-2}, as summarized in **Figure 2e**. However, this low $CaCO_3$ content does not significantly increase the stiffness of hydrogels: E of neat hydrogels is around 23.2 ± 1.4 kPa, whereas that of hydrogels containing 1.2 vol% $CaCO_3$ is around 24.9 ± 1.1 kPa, as shown in **Figure 2a**. These results confirm that the interaction between $CaCO_3$ crystals and PAM hydrogel networks retard the crack initiation within hydrogels under elevated tension and thereby make hydrogels tougher. If we increase the amount of $CaCO_3$ contained in hydrogels to 2.4 vol%, the fracture energy increases to 298.9 ± 51.3 J m^{-2}. Note that a further increase in the mineral content does not increase the fracture energy of hydrogels any more. This observation can be assigned to the decreasing critical extension for the crack initiation that trades off the increasing stiffness of these hydrogels. The decreasing critical extension implies that the incorporation of more $CaCO_3$ crystals hampers their potential to delay crack initiation, even if they offer more interaction sites between $CaCO_3$ crystals and the hydrogel network. This observation might be related to the size of $CaCO_3$ crystals contained in the hydrogels: They have diameters ranging from 3 to 10 μm, as shown in **Figure 2c** and **S7**. This size is significantly larger than the pore size of PAM hydrogel networks, which ranges from 100 nm to 2 μm as shown **Figure 2f** and **S7**. Hence, as $CaCO_3$ crystals form, they introduce defects into the hydrogel network, thereby making it more prone to crack initiation if stretched. As a result of the trade-off between the higher stiffness and smaller critical extension for the crack initiation, the fracture energy of these hydrogels remains similar,

as shown in **Figure 2e**. Our results indicate that the stiffness of our $CaCO_3$-reinforced PAM hydrogels scales with the $CaCO_3$ content. By contrast, their toughness depends on the structure of the hydrogel after mineralization and its interaction with the $CaCO_3$ crystals.

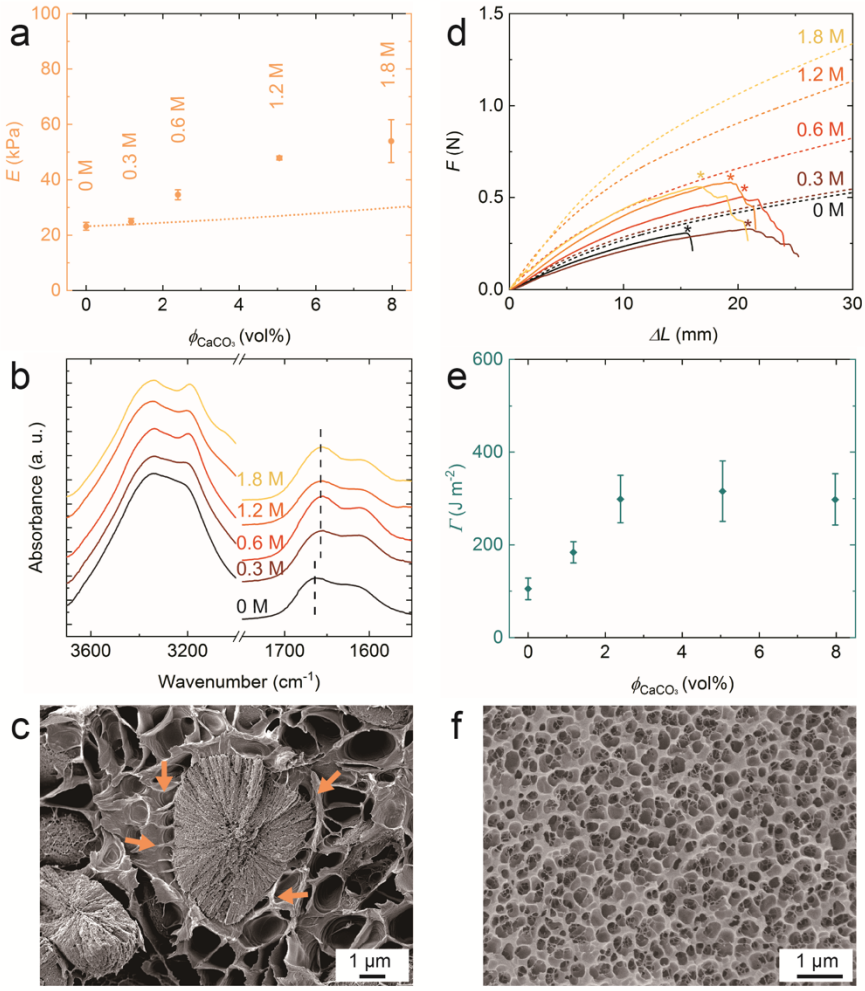

Figure 2. Influence of $CaCO_3$ crystal content. (a) Young's moduli (E) of hydrogels as a function of the volume fraction of $CaCO_3$ minerals (Φ_{CaCO3}) contained in as-prepared hydrogels. The prediction of E for non-interacting filler particles by the Guth-Gold model is shown as dashed line. The initial concentration of $CaCl_2$ contained in the monomer solution is indicated next to the respective sample. (b) FTIR spectra of neat and mineralized PAM hydrogels. (c) Representative SEM image of the hydrogel mineralized with $CaCO_3$ crystals. The connections between the crystals and hydrogel matrix are indicated with arrows. (d) Representative tensile force (F)-extension (ΔL) curves of notched hydrogel samples, indicated as solid lines, and unnotched ones, indicated as dashed lines. The critical extensions corresponding to the crack initiation are marked with asterisks. (e) Fracture energy (Γ) of hydrogels as a function of Φ_{CaCO3}. (f) SEM image of the neat PAM hydrogel.

2.3. Influence of soluble additives

Nature often uses soluble additives, such as amino acids, phosphates and Mg^{2+}, to control the structure of $CaCO_3$ formed in soft matrices and thereby the mechanical properties of the resulting materials.[26–28] Among them, Mg^{2+} is a prominent example that has been extensively used to control the $CaCO_3$ structure in natural and synthetic systems.[28,49] Hence, we employ Mg^{2+} as a model additive to tune the $CaCO_3$ mineralization process within PAM hydrogels. To test the influence of the Mg^{2+} concentration on the structure of the forming minerals, we keep the initial $CaCl_2$ concentration constant at 0.3 M and vary the $MgCl_2$ concentration to obtain Mg/Ca ratios between 1/1 and 5/1. Hydrogels that have been mineralized with Mg/Ca ratios of 1/1 and 2/1 contain a mixture of calcite and nesquehonite ($MgCO_3$ $3H_2O$), as shown in the XRD patterns in **Figure 3a** and FTIR spectra in **Figure S8**. With increasing Mg/Ca ratio, the fraction of amorphous $CaCO_3$ (ACC) increases until we obtain exclusively ACC at a Mg/Ca ratio of 5/1. These results are consistent with those observed for $CaCO_3$ particles formed in bulk aqueous solutions where a sufficiently high amount of Mg^{2+} is known to result in ACC and to stabilize this phase against crystallization.[28,50] The resulting hydrogels display the characteristic peaks of PAM, the C=O stretching around 1656 cm^{-1} and the two split peaks corresponding to the N-H stretching at 3200-3340 cm^{-1}, as shown in **Figure S8**. These peaks are similar to those measured for hydrogels mineralized with $CaCO_3$ crystals in the absence of Mg^{2+}, indicating similar chemical interactions between the PAM and the formed mineral particles. In addition, the morphology of hydrogels mineralized with calcite and $MgCO_3$ $3H_2O$ is similar to that of hydrogels mineralized with $CaCO_3$ crystals in the absence of Mg^{2+}: Big crystals are connected to the surrounding hydrogel network through several polymer fibers, as shown in **Figure 3b** and **S9**. If the Mg/Ca ratio is increased to 3/1 or 4/1, such that the majority of the formed minerals is ACC, we observe particles with average diameters of 869 ± 101 nm and 707 ± 43 nm respectively, as exemplified in **Figure 3c** and **S10**. The size of these particles is significantly smaller than that of crystalline $CaCO_3$ particles. Note that the number of fibers that connect the individual ACC particles to the hydrogel network is higher than what we observe for crystalline counterparts. If the Mg/Ca ratio is further increased to 5/1, the formed ACC particles possess a much smaller average diameter, 459 ± 75 nm. Remarkably, these ACC particles are homogeneously distributed within the hydrogel network and their concentration is sufficiently high to form a percolating structure, in stark contrast to the individual ACC particles observed for Mg/Ca ratios of 3/1 and 4/1, as shown in **Figure 3d** and S10. These results indicate that the size, structure, and morphology of $CaCO_3$ particles formed within the hydrogel, and hence the hydrogel structure, is influenced by the amount of Mg^{2+}.

To test if the size, structure and morphology of $CaCO_3$ influence the mechanical properties of hydrogels, we quantify their Young's moduli and fracture energy. The addition of Mg^{2+} at a Mg/Ca ratio of 1/1 increases the Young's modulus two-fold, as shown in **Figure 3e**. An increase in Mg^{2+} concentration up to a Mg/Ca ratio of 4/1 does not significantly increase the stiffness of the resulting mineralized hydrogels, even though it alters the structure and size of the formed $CaCO_3$. Interestingly, we observe an abrupt increase in the Young's modulus for hydrogels that have been mineralized with a Mg/Ca ratio of 5/1: The stiffness of these hydrogels is approximately 4 times as high as that measured for hydrogels mineralized without Mg^{2+}. These results suggest that the percolating ACC structure that we observe under this condition contributes to the increased stiffness of the hydrogel, in good agreement with recent reports on the hydrogel reinforcement with amorphous calcium phosphate (ACP) nanoparticles[11] and ACC nanoparticles.[41] Similarly, the critical extension for crack initiation in hydrogels mineralized with a Mg/Ca ratio of 5/1 is much higher than that measured for all the other samples, as shown in the force-extension curves in **Figure 3f** and S11. The chemical interactions between the minerals and the hydrogel are independent of the Mg/Ca ratio, as shown in **Figure S8**. Therefore, we attribute the strong increase in the critical extension to the percolating ACC network that forms if a sufficient quantity of Mg^{2+} is present. This mineral-based percolating network distributes the applied stress over a wider area around the notch, thereby delaying the crack initiation.[51] As a result of the significantly higher stiffness and larger critical extension, the fracture energy of these hydrogels is as high as 1303.7 ± 337.0 J m^{-2}, a value similar to that measured for double-network hydrogels.[9] Hence, the percolating ACC network increases the stiffness of the neat PAM hydrogel four-fold and the fracture energy by a factor of 13. This reinforcement is much more effective than that provided by $CaCO_3$ crystals that form in the absence of Mg^{2+}.

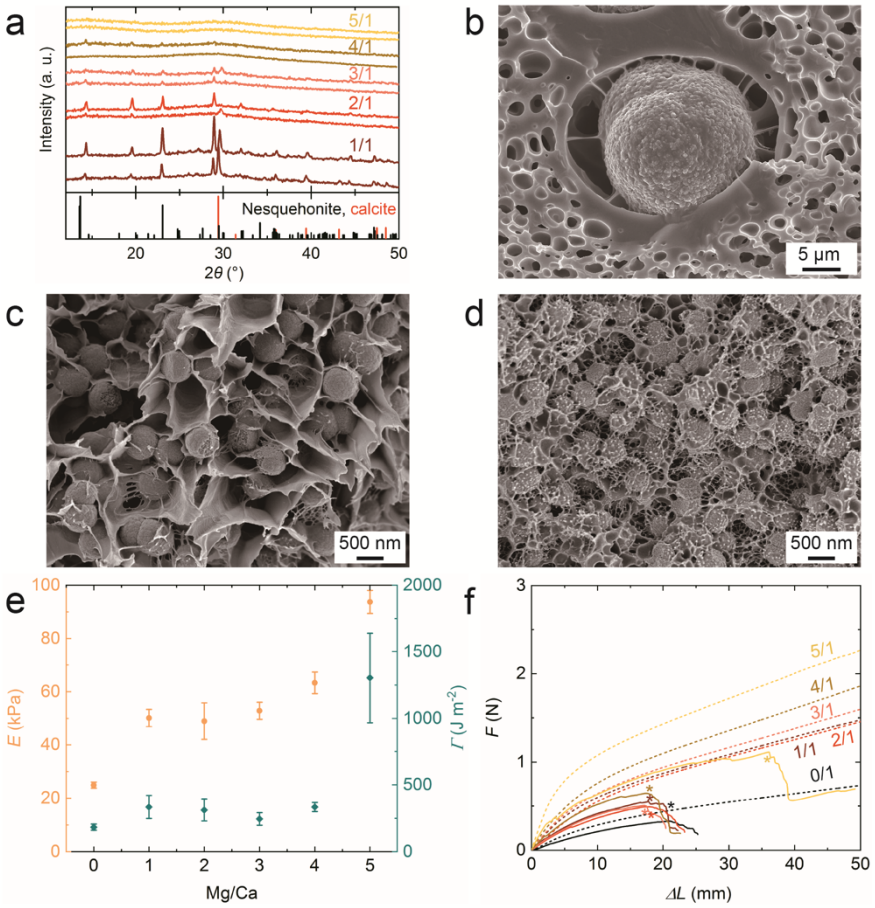

Figure 3. Influence of the soluble additive Mg^{2+}. (a) Representative XRD patterns of mineralized hydrogels produced from monomer solutions containing 0.3 M $CaCl_2$ and different concentrations of $MgCl_2$. The Mg/Ca ratios are labelled next to the corresponding curves. (d-f) SEM images of mineralized hydrogels produced with Mg/Ca ratios of (b) 2/1, (c) 4/1 and (d) 5/1. (f) Young's moduli (E) and fracture energy (Γ) of hydrogels as a function of the Mg/Ca ratio. (f) Force (F)-extension (ΔL) curves of notched mineralized hydrogels, indicated as solid lines, and unnotched ones, indicated as dashed lines.

2.4. Influence of functionalization of hydrogel matrix

Surfaces of natural soft tissues often contain proteins possessing certain functional groups with a high affinity to Ca^{2+}, such as carboxylic groups.[26,27,52] These functional groups have been shown to control the size, morphology, crystallinity and orientation of the formed $CaCO_3$ during the biomineralization and hence the mechanical properties of resulting $CaCO_3$-containing materials.[26,27,52,53] To study how the functional group of PAM influences the $CaCO_3$ mineralization in our work, we replace part of the acrylamide monomers with acrylic acid (AA) to form a covalently crosslinked PAM-co-PAA (w/w = 85/15) hydrogel that acts as the matrix for the mineralization. Similar to the PAM hydrogels mineralized with $CaCO_3$ crystals, the PAM-co-PAA hydrogels produced from a monomer solution containing 1.8 M $CaCl_2$ also comprise a mixture of vaterite and calcite, as shown in the **Figure S12** and **S13**. However, crystals formed in the PAM-co-PAA matrix are larger, with diameters ranging from 20 μm to 40 μm, and more spherical than those formed in PAM hydrogels, as shown in **Figure 4a** and **S14**. These results are in good agreement with a previous report suggesting that the functionalization of AA favors the spherulitic growth of large crystals.[54] By contrast, the functionalization of AA does not influence the structure of $CaCO_3$ if formed in the presence of Mg^{2+} with a Mg/Ca ratio of 5/1: the resulting minerals are still ACC, as confirmed by the XRD pattern in **Figure S12** and the FTIR spectra in **Figure S13**.

Acrylic acid is known to increase the affinity of the matrix towards $CaCO_3$ crystals[27,52] such that we expect the crystals to be better connected to the hydrogel network. Indeed, we observe more and tighter connections between the crystal surfaces and the hydrogel after the PAM hydrogel has been functionalized with AA: the $CaCO_3$ crystals are fully attached to the surrounding hydrogel network, as shown in **Figure 4a**. Acrylic acid changes the hydrogel/mineral interface even more if $CaCO_3$ forms in the presence of Mg^{2+}: These ACC minerals are highly percolating agglomerates composed of small clusters with sizes ranging from a few 10s nm to 100 nm, as shown in **Figure 4b** and **S15**. In certain regions of the mineralized hydrogels especially those containing a lower density of ACC agglomerates, the hydrogel network is coated with a layer of ACC, as illustrated in **Figure 4b-d** and **S15**. These results are similar to those reported for the mineralization of cellulose acetate microfibers, in which the microfibers are coated with a uniform $CaCO_3$ layer rather than randomly distributed crystals if functionalized with PAA.[55] The formation of a mineral coating on the hydrogel network is likely caused by the small size of ACC clusters and their high affinity towards the hydrogel chains offered by the functionalization with AA.

Our results suggest that the size and morphology of $CaCO_3$ formed within hydrogels changes if the hydrogels are functionalized with AA. To test if these factors influence the mechanical properties of the resulting mineralized hydrogels, we quantify the Young's moduli and fracture energy of mineralized PAM-co-PAA and compare these values to those measured for PAM hydrogels. Neat PAM-co-PAA hydrogels display a similar Young's modulus and fracture energy to the neat PAM hydrogel, indicating that the functionalization of PAM with 15wt% AA does not significantly change the mechanical properties of the hydrogels, as summarized in **Figure 4e**. The functionalization of hydrogels with AA slightly increases their Young's modulus from 54.0 ± 7.7 kPa to 63.7 ± 1.5 kPa if mineralized with $CaCO_3$ crystals. This increase in stiffness is likely caused by the stronger hydrogel-mineral interactions, as shown in **Figure 4a**. However, the functionalization with AA decreases the facture energy of these hydrogels from 298.1 ± 55.3 J m^{-2} to 157.8 ± 30.4 J m^{-2}. This reduction might be caused by the bigger size of crystals formed in PAA-co-PAM hydrogels that introduce more defects into the hydrogel network. Interestingly, the increase in stiffness upon functionalization with AA is much more pronounced if the hydrogel is mineralized with ACC: the Young's modulus increases 12-fold from 93.7 ± 4.3 kPa to 1145.7 ± 467.0 kPa whereas its fracture energy decreases only approximately 2-fold from 1303.7 ± 337.0 J m^{-2} to 686.0 ± 231.0 J m^{-2}, as shown in **Figure 4e**. Hence, the stiffness of the PAM-co-PAA hydrogel increases more than 50 times if reinforced with ACC whereas its fracture energy is approximately 6 times higher.

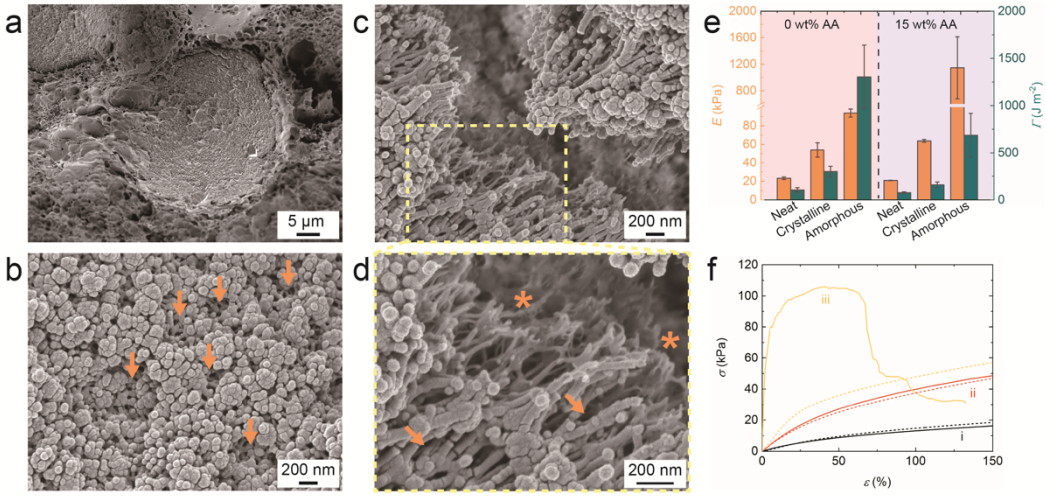

Figure 4. Influence of the functionalization of PAM hydrogels with acrylic acid (AA). (a-e) SEM images of mineralized PAM-co-PAA hydrogels produced from monomer solutions containing (a) 1.8 M $CaCl_2$ and (b-d) 0.3 M $CaCl_2$ and 1.5 M $MgCl_2$. The mineral coating layers formed on the hydrogel network are indicated with arrows and the neat hydrogel network with asterisks. (e) Comparison of Young's moduli (E) and fracture energy (Γ) of PAM-based hydrogels and PAM-co-PAA counterparts. (f) Stress (σ)-strain (ε) curves measured on PAM

hydrogels, marked as dotted lines and PAM-co-PAA hydrogels, marked as solid lines. Hydrogels are produced from monomer solutions containing (i) no $CaCl_2$ or $MgCl_2$ (ii) 1.8 M $CaCl_2$ and (iii) 0.3 M $CaCl_2$ and 1.5 M $MgCl_2$.

To investigate the reason for the remarkable enhancement in the stiffness observed for PAM-co-PAA hydrogels mineralized with ACC, we test if an ionically crosslinked network forms by the complexation of the acrylic group with Ca^{2+} and Mg^{2+}. Indeed, certain metal cations, such as Fe^{3+} and Ca^{2+}, have been reported to favor the formation of an ionically crosslinked hydrogel network via their complexation with acrylic groups contained in hydrogels, thereby significantly enhancing the mechanical properties of hydrogels.[14,56,57] To test if the AA-cation complexation influences the mechanical properties of our hydrogels, we prepare non-mineralized PAM-co-PAM hydrogels containing 1.8 M NaCl, in which no complexation between Na^{2+} and carboxylic groups can occur. We compare their mechanical properties to those containing 1.8 M Ca^{2+} and 0.3 M Ca^{2+}/1.5 M Mg^{2+}. All three types of hydrogels display similar mechanical properties, as shown in **Figure S16**. This result indicates that the ionically crosslinked network between acrylic groups and Ca^{2+} or Mg^{2+} contained in our hydrogels is unlikely to form and hence, to contribute to the increased stiffness. Instead, we assign the remarkable increase in stiffness to the formation of the mineral coating layer on the hydrogel network and the percolating mineral network composed of smaller ACC clusters. The small mineral clusters are expected to be better integrated into the hydrogel network, consistent with a report on PAM hydrogels mineralized with ACP particles.[58] However, the mineral-coated hydrogel network is more rigid and displays a reduced stretchability, as illustrated in the stress-strain curves in **Figure 4f**. As a result of the much lower stretchability, these hydrogels display a smaller fracture energy compared to the mineralized PAM counterparts. Hence, our results demonstrate that the functionalization of PAM hydrogels with AA significantly broadens the range of mechanical properties that can be achieved by reinforcing hydrogels with $CaCO_3$.

3. Conclusion

Calcium carbonate biominerals that display different sizes, structures and morphologies are often the structural components in living organisms, yet the influence of these factors on the mechanical properties of the resulting biomaterials is still poorly understood.[26,31,59,60] We demonstrate that these factors also strongly influence the overall mechanical properties of the mineralized hydrogels. For example, reinforcing hydrogels with large individual $CaCO_3$ crystals enhances their toughness three-fold whereas the reinforcement with small percolating ACC nanoparticles increases it 13-fold. These results hint at the importance of the size, structure

and morphology of $CaCO_3$ minerals in living organisms for the mechanical properties and structural function of the resulting biomineral-based materials. Moreover, we exemplify the power of soluble additives and the hydrogel functionalization in controlling the size, structure and morphology of $CaCO_3$ and hence, the mechanical properties of mineralized hydrogels: The stiffness hydrogels increases up to 50-fold if functionalized with acrylic acid and reinforced with a percolating network of ACC particles that forms in the presence of sufficient amounts of Mg^{2+}. The structure of $CaCO_3$ as well as additives contained in it have been shown to significantly influence the bioactivity and biodegradability of $CaCO_3$.[21,22,24,60] Taking advantage of this knowhow, our work might open up new opportunities to fabricate strong and tough $CaCO_3$-reinforced functional materials.

4. Experimental Section

Preparation of mineralized hydrogels

To produce PAM hydrogels mineralized with $CaCO_3$ crystals, we premix $CaCl_2$ (anhydrous, Carl Roth) with an aqueous hydrogel precursor solution that contains 20 wt% acrylamide (AM, Sigma-Aldrich) monomer, 0.1 mol% N,N'-Methylenebisacrylamide (MBAA, Carl Roth) used as a crosslinker and 0.1 mol% 2-Hydroxy-4′-(2-hydroxyethoxy)-2-methylpropiophenone (Irgacure 2959, Sigma-Aldrich) that is a photo-initiator. The mixture is poured into a Teflon mold (30 mm × 15 mm × 2 mm) that is covered with glass slides and subsequently crosslinked using UV light (UVP CL-1000, Analytik Jena, 365 nm, 2 mW cm^{-2}) for 15 min. To study the influence of Mg^{2+}, the indicated amount of $MgCl_2$ (hexahydrate, Carl Roth) is also added to the above-mentioned mixture prior to the UV-initiated crosslinking. To functionalize the PAM hydrogels with acrylic acid, we replace the 20 wt% acrylamide with a mixture of 17 wt% acrylamide and 3 wt% acrylic acid (Sigma-Aldrich). The pH of the acrylic acid solution is adjusted to around 6, similar to that of the acrylamide solution, by titrating with a NaOH solution.

The covalently crosslinked hydrogels are mineralized in a well-sealed petri dish. Hydrogels are placed on top of two plastic micro spatulas to ensure that most of their surfaces are exposed to the ambient atmosphere. A small petri dish containing 5 mL DI-water is put in the chamber to avoid dehydration of the hydrogels, as demonstrated in the Table S1. Another small petri dish containing 3 g ammonium carbonate powder ($(NH_4)_2CO_3$ (Sigma-Aldrich)) is put next to the hydrogel. The ammonium carbonate powder decomposes into CO_2 and NH_3 gases. While the dissolution of CO_2 in water contained in hydrogels forms carbonic acid (H_2CO_3), the dissolution of NH_3 produces $NH_3{\cdot}H_2O$.[61] The increase in pH of the mineralization solution caused by

$NH_3 \cdot H_2O$ deprotonates carbonic acids to form CO_3^{2-} ions and thereby initiates the formation of $CaCO_3$ minerals. Hydrogels are left in the reaction chamber at room temperature for 4 days to ensure a complete conversion of $CaCl_2$ into $CaCO_3$ minerals.

Characterizations

Single edge notch tensile test: Single edge notch tensile tests are conducted using a commercial uniaxial testing machine (ZwickiLine 5 kN, Zwick Roell, 100 N load cell). Cuboidal hydrogel samples (30 mm × 15 mm × 2 mm) are mounted between two metallic clamps with a distance of 20 mm. Samples are preloaded with 0.005 N and are stretched at a constant velocity of 100 mm min^{-1}. The measurement is automatically stopped once the measured force falls below 80% of the maximum applied force. For each notched hydrogel sample, a 7.5 mm long notch is cut into the hydrogel using a scissor. To better assess the toughness of hydrogels, we quantify their fracture energy from the force-extension curves of notched and unnotched samples, as detailed in the Figure S5. The results obtained with this method have been shown to be very reproducible since it is insensitive to defects already present in the hydrogel or caused by the clamps during stretching.[14] *Fourier-transform infrared spectroscopy (FTIR):* FITR spectra are acquired on as-prepared hydrogels samples using a Nicolet 6700 FTIR spectrometer (ThermoFisher Scientific) operated in the attenuated total reflection (ATR) mode. *X-ray diffraction (XRD):* XRD patterns are acquired on as-prepared samples using an Empyrean diffractometer (Malvern Panalytical) at a scanning rate of 0.1° s^{-1}. *Thermogravimetric analysis (TGA):* TGA measurements are performed with a TGA 4000 instrument (Perkin Elmer). To avoid the influence of any soluble salts contained in the hydrogel, all the hydrogels are washed thoroughly with deionized water and subsequently dried at 60 ℃ in the oven overnight. For each measurement, approximately 5 to 10 mg of dry hydrogel is placed into an alumina crucible. The crucible is heated from 30 ℃ to 850 ℃ at a rate of 10 ℃ min^{-1} under a flow of dry nitrogen or air with a flow rate of 20 ml min^{-1}. *Scanning electron microscopy (SEM):* The morphology of neat and mineralized hydrogels is characterized using a scanning electron microscope (Zeiss Merlin and Zeiss Gemini) with an Inlens detector. To avoid artifacts from soluble salts contained in the mineralized hydrogels, we wash the mineralized hydrogels with an excess of solvent before drying them in air. To minimize the effect of solvent on the swelling of the hydrogel networks and alteration of minerals during washing as well as to ensure a good solubility of salts within it, we employ methanol (Carl Roth) to wash our hydrogels. The washed mineralized hydrogels are dried at room temperature in air. Dry samples are fractured into small pieces to expose the cross-section of hydrogels to methanol during a second washing procedure, which is the same as described above. To measure the pore size of neat hydrogels, the freshly

prepared neat hydrogels are frozen using liquid nitrogen and subsequently dried with a freeze-dryer (Labconco, FreeZone 2.5). To better visualize the distribution of $CaCO_3$ crystals in hydrogels, certain hydrogels mineralized with crystalline $CaCO_3$ are washed with water and subsequently dried at 60 ℃ overnight so that the hydrogel networks collapse into a dense matrix. The cross-sections of these dried samples are exposed and polished using a mechanical polisher (Milian Dutscher Group, 420CA). All the samples investigated with SEM are coated with a conductive 10 nm Au:Pd (80/20) or 6 nm Pt:Pd (80/20) film to avoid charging effects.

Supporting Information

Supporting Information is available from the Wiley Online Library or from the author.

Acknowledgements

We thank Dr. Wenhua Bi and Yueyue Bao for their valuable support for our project. This work was financially supported by the Swiss National Center of Competence in Research (NCCR) Bio-Inspired Materials (51NF40-182881).

Received: ((will be filled in by the editorial staff))
Revised: ((will be filled in by the editorial staff))
Published online: ((will be filled in by the editorial staff))

References

[1] Y. S. Zhang, A. Khademhosseini, *Science* **2017**, *356*, eaaf3627.

[2] N. Annabi, A. Tamayol, J. A. Uquillas, M. Akbari, L. E. Bertassoni, C. Cha, G. Camci-Unal, M. R. Dokmeci, N. A. Peppas, A. Khademhosseini, *Advanced Materials* **2014**, *26*, 85.

[3] H. Yuk, B. Lu, X. Zhao, *Chem. Soc. Rev.* **2019**, *48*, 1642.

[4] A. Jayakumar, V. K. Jose, J.-M. Lee, *Small Methods* **2020**, *4*, 1900735.

[5] Z. Wang, H. Li, Z. Tang, Z. Liu, Z. Ruan, L. Ma, Q. Yang, D. Wang, C. Zhi, *Advanced Functional Materials* **2018**, *28*, 1804560.

[6] H. Fan, J. P. Gong, *Macromolecules* **2020**, *53*, 2769.

[7] T. Sakai, T. Matsunaga, Y. Yamamoto, C. Ito, R. Yoshida, S. Suzuki, N. Sasaki, M. Shibayama, U. Chung, *Macromolecules* **2008**, *41*, 5379.

[8] Y. Okumura, K. Ito, *Advanced Materials* **2001**, *13*, 485.

[9] J. P. Gong, Y. Katsuyama, T. Kurokawa, Y. Osada, *Advanced Materials* **2003**, *15*, 1155.

[10] K. Haraguchi, T. Takehisa, *Advanced Materials* **2002**, *14*, 1120.

[11] N. Rauner, M. Meuris, M. Zoric, J. C. Tiller, *Nature* **2017**, *543*, 407.

[12] J. Hu, K. Hiwatashi, T. Kurokawa, S. M. Liang, Z. L. Wu, J. P. Gong, *Macromolecules* **2011**, *44*, 7775.

[13] S. Lin, C. Cao, Q. Wang, M. Gonzalez, J. E. Dolbow, X. Zhao, *Soft Matter* **2014**, *10*, 7519.

[14] J.-Y. Sun, X. Zhao, W. R. K. Illeperuma, O. Chaudhuri, K. H. Oh, D. J. Mooney, J. J. Vlassak, Z. Suo, *Nature* **2012**, *489*, 133.

[15] W.-C. Lin, W. Fan, A. Marcellan, D. Hourdet, C. Creton, *Macromolecules* **2010**, *43*, 2554.

[16] T. Huang, H. G. Xu, K. X. Jiao, L. P. Zhu, H. R. Brown, H. L. Wang, *Advanced Materials* **2007**, *19*, 1622.

[17] N. Rauner, M. Meuris, S. Dech, J. Godde, J. C. Tiller, *Acta Biomaterialia* **2014**, *10*, 3942.

[18] N. Rauner, L. Buenger, S. Schuller, J. C. Tiller, *Macromolecular Rapid Communications* **2015**, *36*, 224.

[19] M. Guvendiren, P. A. Heiney, S. Yang, *Macromolecules* **2009**, *42*, 6606.

[20] S. Sun, L.-B. Mao, Z. Lei, S.-H. Yu, H. Cölfen, *Angewandte Chemie International Edition* **2016**, *55*, 11765.

[21] X. Wu, S. I. Stroll, D. Lantigua, S. Suvarnapathaki, G. Camci-Unal, *Biomaterials Science* **2019**, *7*, 2675.

[22] T. E. L. Douglas, A. Łapa, S. K. Samal, H. A. Declercq, D. Schaubroeck, A. C. Mendes, P. V. der Voort, A. Dokupil, A. Plis, K. D. Schamphelaere, I. S. Chronakis, E. Pamuła, A. G. Skirtach, *Journal of Tissue Engineering and Regenerative Medicine* **2017**, *11*, 3556.

[23] Y. Suzawa, T. Funaki, J. Watanabe, S. Iwai, Y. Yura, T. Nakano, Y. Umakoshi, M. Akashi, *Journal of Biomedical Materials Research Part A* **2010**, *93A*, 965.

[24] R. Schröder, L. Besch, H. Pohlit, M. Panthöfer, W. Roth, H. Frey, W. Tremel, R. E. Unger, *Journal of Tissue Engineering and Regenerative Medicine* **2018**, *12*, 1754.

[25] M. A. E. Cruz, G. C. M. Ruiz, A. N. Faria, D. C. Zancanela, L. S. Pereira, P. Ciancaglini, A. P. Ramos, *Applied Surface Science* **2016**, *370*, 459.

[26] L. Addadi, D. Joester, F. Nudelman, S. Weiner, *Chemistry - A European Journal* **2006**, *12*, 980.

[27] L. B. Gower, *Chemical Reviews* **2008**, *108*, 4551.

[28] H. Du, E. Amstad, *Angewandte Chemie International Edition* **2020**, *59*, 1798.

[29] W. Huang, D. Restrepo, J. Jung, F. Y. Su, Z. Liu, R. O. Ritchie, J. McKittrick, P. Zavattieri, D. Kisailus, *Adv. Mater.* **2019**, 1901561.

[30] U. G. K. Wegst, H. Bai, E. Saiz, A. P. Tomsia, R. O. Ritchie, *Nature Materials* **2015**, *14*, 23.

[31] J. C. Weaver, G. W. Milliron, A. Miserez, K. Evans-Lutterodt, S. Herrera, I. Gallana, W. J. Mershon, B. Swanson, P. Zavattieri, E. DiMasi, D. Kisailus, *Science* **2012**, *336*, 1275.

[32] A. Finnemore, P. Cunha, T. Shean, S. Vignolini, S. Guldin, M. Oyen, U. Steiner, *Nature Communications* **2012**, *3*.

[33] L.-B. Mao, H.-L. Gao, H.-B. Yao, L. Liu, H. Colfen, G. Liu, S.-M. Chen, S.-K. Li, Y.-X. Yan, Y.-Y. Liu, S.-H. Yu, *Science* **2016**, *354*, 107.

[34] T. Saito, Y. Oaki, T. Nishimura, A. Isogai, T. Kato, *Materials Horizons* **2014**, *1*, 321.

[35] E. Asenath-Smith, H. Li, E. C. Keene, Z. W. Seh, L. A. Estroff, *Advanced Functional Materials* **2012**, *22*, 2891.

[36] C. Kosanović, G. Falini, D. Kralj, *Crystal Growth & Design* **2011**, *11*, 269.

[37] J. Xiao, S. Yang, *Nanoscale* **2012**, *4*, 54.

[38] N. Gehrke, N. Nassif, N. Pinna, M. Antonietti, H. S. Gupta, H. Cölfen, *Chemistry of Materials* **2005**, *17*, 6514.

[39] X. Cheng, L. B. Gower, *Biotechnology Progress* **2006**, *22*, 141.

[40] T. Sakamoto, A. Oichi, Y. Oaki, T. Nishimura, A. Sugawara, T. Kato, *Crystal Growth & Design* **2009**, *9*, 622.

[41] M. Milovanovic, L. Mihailowitsch, M. Santhirasegaran, V. Brandt, J. C. Tiller, *J Mater Sci* **2021**, 56, 15299.

[42] W.-C. Lin, A. Marcellan, D. Hourdet, C. Creton, *Soft Matter* **2011**, *7*, 6578.

[43] S. Kim, A. U. Regitsky, J. Song, J. Ilavsky, G. H. McKinley, N. Holten-Andersen, *Nature Communications* **2021**, *12*, 667.

[44] H. Jiang, G. Zhang, F. Li, Y. Zhang, Y. Lei, Y. Xia, X. Jin, X. Feng, H. Li, *Nanoscale* **2017**, *9*, 15470.

[45] M. K. Pal, J. Gautam, *Polymer Composites* **2012**, *33*, 515.

[46] K. Haraguchi, M. Ebato, T. Takehisa, *Advanced Materials* **2006**, *18*, 2250.

[47] X. Zhao, *Soft Matter* **2014**, *10*, 672.

[48] M. Morits, T. Verho, J. Sorvari, V. Liljeström, M. A. Kostiainen, A. H. Gröschel, O. Ikkala, *Advanced Functional Materials* **2017**, *27*, 1605378.

[49] L. Addadi, S. Raz, S. Weiner, *Advanced Materials* **2003**, *15*, 959.

[50] R. S. K. Lam, J. M. Charnock, A. Lennie, F. C. Meldrum, *CrystEngComm* **2007**, *9*, 1226.

[51] Q. Wang, R. Hou, Y. Cheng, J. Fu, *Soft Matter* **2012**, *8*, 6048.

[52] N. A. J. M. Sommerdijk, G. de With, *Chemical Reviews* **2008**, *108*, 4499.

[53] H. Du, U. Steiner, E. Amstad, *CHIMIA International Journal for Chemistry* **2019**, *73*, 29.

[54] O. Grassmann, P. Löbmann, *Biomaterials* **2004**, *25*, 277.

[55] L. Liu, D. He, G.-S. Wang, S.-H. Yu, *Langmuir* **2011**, *27*, 7199.

[56] P. Lin, S. Ma, X. Wang, F. Zhou, *Advanced Materials* **2015**, *27*, 2054.

[57] X. Li, H. Wang, D. Li, S. Long, G. Zhang, Z. Wu, *ACS Appl. Mater. Interfaces* **2018**, *10*, 31198.

[58] Y. Yu, Z. Mu, B. Jin, Z. Liu, R. Tang, *Angew. Chem. Int. Ed.* **2020**, *59*, 2071.

[59] S. Amini, A. Masic, L. Bertinetti, J. S. Teguh, J. S. Herrin, X. Zhu, H. Su, A. Miserez, *Nature Communications* **2014**, *5*, 3187.

[60] B. Cantaert, D. Kuo, S. Matsumura, T. Nishimura, T. Sakamoto, T. Kato, *ChemPlusChem* **2017**, *82*, 107.

[61] J. Ihli, P. Bots, A. Kulak, L. G. Benning, F. C. Meldrum, *Advanced Functional Materials* **2013**, *23*, 1965.

We study the reinforcing effect of $CaCO_3$ minerals on hydrogels by systematically tuning the content, size, structure, and distribution of $CaCO_3$ contained in them. We demonstrate that the reinforcement is most efficient if small amorphous $CaCO_3$ particles form a percolating network that strongly interacts with the hydrogel matrix.

Huachuan Du, Tianyu Yuan, Ran Zhao, Matteo Hirsch, Michael Kessler, Esther Amstad*

Biomineralization-inspired reinforcement of hydrogels